Final version published as Science Signaling 8 (364): ra19 (2015). DOI: 10.1126/scisignal.2005672

Plasma membrane Ca^{2+}-ATPases can shape the pattern of Ca^{2+} transients induced by store-operated Ca^{2+} entry

Katalin Pászty[1], Ariel J. Caride[2], Željko Bajzer[3,4], Chetan P. Offord[5], Rita Padányi[6,8], Luca Hegedűs[7], Karolina Varga[7,8], Emanuel E. Strehler[4], Agnes Enyedi[6,7,8]*

[1]Molecular Biophysics Research Group of the Hungarian Academy of Sciences and Department of Biophysics, Semmelweis University, Budapest, Hungary

[2]Hematology Research, Mayo Clinic, Rochester MN, USA

[3]Department of Physiology and Biomedical Engineering, Division of Biomathematics, Mayo Clinic, College of Medicine, Rochester MN, USA

[4]Department of Biochemistry and Molecular Biology, Mayo Clinic College of Medicine, Rochester, MN, USA

[5]Molecular Medicine Program, Mayo Clinic College of Medicine, Rochester MN USA

[6]Hungarian National Blood Transfusion Service, Budapest, Hungary

[7]Institute of Molecular Pharmacology, Research Centre for Natural Sciences, Hungarian Academy of Sciences, Budapest, Hungary

[8] 2nd Department of Pathology, Semmelweis University, Budapest, Hungary

*To whom correspondence should be addressed: E-mail: enyedi@biomembrane.hu

Abstract

Calcium (Ca^{2+}) is a critical cofactor and signaling mediator in cells and the concentration of cytosolic Ca^{2+} is regulated by multiple proteins, including the plasma membrane Ca^{2+}-ATPases (PMCAs), which use ATP to transport Ca^{2+} out of cells. PMCA isoforms exhibit different kinetic and regulatory properties, thus the presence and relative abundance of individual isoforms may help shape Ca^{2+} transients and cellular responses. We studied the effects of three PMCA isoforms (PMCA4a, PMCA4b, PMCA2b) on Ca^{2+} transients elicited by conditions that trigger store-operated Ca^{2+} entry (SOCE) and that blocked Ca^{2+} uptake into the endoplasmic reticulum in HeLa cells, human embryonic kidney (HEK) 293 cells, or primary endothelial cell isolated from human umbilical cord veins (HUVECs). The slowly activating PMCA4b isoform produced long-lasting Ca^{2+} oscillations in response to SOCE. The fast-activating isoforms PMCA2b and PMCA4a produced different effects. PMCA2b resulted in rapid and highly PMCA abundance-sensitive clearance of SOCE-mediated Ca^{2+} transients; whereas PMCA4a reduced cytosolic Ca^{2+} resulting in the establishment of a higher than baseline cytosolic Ca^{2+} concentration. Mathematical modeling showed that slow activation was critical to the sustained oscillation induced by the "slow" PMCA4b pump. The modeling and experimental results indicated that the distinct properties of PMCA isoforms differentially regulate the pattern of SOCE-mediated Ca^{2+} transients, which would thus affect the activation of downstream signaling pathways.

Introduction

Different types of stimuli evoke Ca^{2+} release from the endoplasmic reticulum (ER) Ca^{2+} stores through inositol 3-phosphate (IP_3) receptors, which are ligand-activated Ca^{2+} channels. When ER Ca^{2+} is diminished, STIM (stromal interaction molecule; STIM 1 and 2) molecules aggregate in the ER membrane and translocate to regions near the plasma membrane where they

activate ORAI (ORAI 1, 2, and 3), the pore forming subunits of store-operated calcium entry (SOCE) channels *(1-3)*. Several downstream pathways are regulated by Ca^{2+} entry through SOCE rather than by Ca^{2+} released from internal stores *(4-8)*. SOCE stimulates the calcium-regulated phosphatase calcineurin, which activates the transcription factor NFAT *(9, 10)*, stimulates or inhibits adenylyl cyclases *(5)*, stimulates transcription of the early gene, *cfos (4)*, and activates cytoplasmic phospholipase A_2 ($cPLA_2$) *(4, 11)*.

Following an increase in cytosolic Ca^{2+} concentration ($[Ca^{2+}]_i$), "excess" Ca^{2+} that is not buffered is removed from the cytoplasm by a combination of activities of plasma membrane transporters [Na^+-Ca^{2+} exchanger (NCX) and Ca^{2+} ATPase pumps (PMCAs)], the mitochondrial Ca^{2+} uniporter, and the sarcoplasmic or endoplasmic reticulum (SERCA) and the secretory pathway (SPCA) Ca^{2+} ATPase pumps *(12)*. Ca^{2+}-activated cell functions depend on the amplitude and the spatial and temporal shape of the Ca^{2+} signal; hence, modulation of the signal by Ca^{2+}-removal mechanisms is predicted to impact the cellular response.

PMCAs are key elements of the cytosolic Ca^{2+}-removal system. There are four genes encoding mammalian PMCAs (PMCA1-4) and alternative splicing generates more than 20 PMCA variants *(13)*. Although all PMCAs are activated by Ca^{2+}-calmodulin (CaM), they differ in the kinetics of activation by and affinity for Ca^{2+}-CaM. Here, we focus on 3 isoforms: PMCA2b, PMCA4b, and PMCA4a (Table 1). The kinetics of binding (k_{on}) of Ca^{2+}-CaM to PMCA4b are very slow; whereasPMCA2b and PMCA4a exhibit fast Ca^{2+}-CaM binding *(14-17)*. The inactivation rates of the pumps are also different with PMCA2b and PMCA4b remaining active much longer than PMCA4a, which has a much faster Ca^{2+}-CaM off rate (k_{off}) *(14, 18, 19)*. This long-lasting activity of PMCA2b and PMCA4b has been referred to as a "memory" of a past Ca^{2+} spike *(19)*. It is also important to note that PMCA2b has the longest memory of all PMCAs (Table 1). The differences in their kinetics imply that each PMCA isoform will respond

differently to an incoming Ca^{2+} signal. Therefore, we speculated that each cell type has the appropriate set of PMCA isoforms such that cells that need to respond quickly to an incoming spike (for example, neurons) will have "fast" pumps and non-excitable cells will have "slow" pumps *(18)*. PMCA4 is ubiquitously distributed; PMCA4b is the major isoform of human erythrocytes, as well as of many epithelial cells such as in the kidney *(20)*; whereas PMCA2b and PMCA4a are present in specific areas of the brain and other highly specialized cells and tissues *(21)*.

Data comparing the influence of different PMCA isoforms on the cytosolic Ca^{2+} signaling of live cells are limited. Experiments with Chinese hamster ovary (CHO) cells in which IP_3-mediated Ca^{2+} release from internal stores was measured together with Ca^{2+} entry through plasma membrane channels, and PMCA isoforms were overexpressed, the ubiquitously distributed PMCA isoforms PMCA1 and PMCA4 were less effective in Ca^{2+} clearance than the specialized "fast" pumps PMCA2 and 3 *(22, 23)*. The faster clearance was attributed to the increased exporting activity of the PMCA2 and PMCA3 isoforms, and the differences in peak of the Ca^{2+} signal were ascribed to differences in either ER Ca^{2+} content or the efficiency of Ca^{2+} extrusion. However, most of these experiments examined global Ca^{2+} changes and only a few examined specifically the SOCE-mediated Ca^{2+} signals *(22, 24-28)*.

The Ca^{2+} signal initiated by SOCE is tuned by several mechanisms that finally determine the extent (in time and space) of the Ca^{2+} signal, which is then translated into different downstream events. Here, we examined how PMCA4a, PMCA4b, and PMCA2b, which have different activation and inactivation kinetics (Table 1), affected Ca^{2+} transients mediated by SOCE. We established a HeLa cell line in which PMCA4 was stably knocked down, expressed mCherry-tagged PMCA variants of PMCA4a, PMCA4b, or PMCA2b, and measured the SOCE-induced Ca^{2+} signal by coexpressing the genetically-encoded Ca^{2+} indicator GCaMP2. We then developed

a simplified model that included specific kinetic features of the PMCAs and used the model to explore how the kinetic parameters of PMCA4b produced an oscillating Ca^{2+} signal in response to SOCE. The model also correctly replicated the experimentally observed SOCE-induced Ca^{2+} signal in cells expressing PMCA2b or PMCA4a and may thus be useful for predicting the pattern of Ca^{2+} signaling in cells containing different amounts and types of the PMCA pumps.

Results

SOCE-mediated Ca^{2+} signals are more uniform in PMCA4-knockdown HeLa cells than in wild-type HeLa cells.

Cytosolic calcium transients are shaped by complex mechanisms, including Ca^{2+} influx through plasma membrane channels, Ca^{2+} release from intracellular stores, and multiple calcium-removal systems. To understand how different PMCA isoforms influence Ca^{2+} signaling, we examined their effects on the Ca^{2+} transients generated by SOCE. We found that HeLa cells had relatively small amounts of PMCA1 and PMCA4b isoforms and that the abundance of PMCA4b increased when cells reached confluence (Fig. 1A). We had previously generated a stable HeLa cell line (sh-PMCA4) in which PMCA4 isoforms were knocked down with a short-hairpin RNA against PMCA4 *(29)* and we confirmed that this line lacked PMC4b in subconfluent and confluent cultures (Fig. 1A). We transiently transfected the sh-PMCA4 and wild-type HeLa cells with the fluorescent calcium indicator GCaMP2 and monitored Ca^{2+} signals in confluent cultures in response to SOCE using a Ca^{2+} re-addition protocol under conditions in which Ca^{2+} uptake into the ER was blocked with thapsigargin (Fig. 1B). To activate SOCE, we emptied the ER Ca^{2+} pool under nominally Ca^{2+}-free conditions by the sequential additions of thapsigargin (to specifically inhibit SERCA) and ATP. In some experiments, we used thapsigargin in combination with low concentrations of the Ca^{2+} ionophore ionomycin, which primarily releases Ca^{2+} from the internal pool *(30)*. After releasing Ca^{2+} from the ER pool in Ca^{2+}-free medium, re-addition of Ca^{2+} to the

medium resulted in a large increase in $[Ca^{2+}]_i$ that persisted for about 10-15 minutes in both the sh-PMCA4 and control HeLa cells (Fig. 1C, D). The sh-PMCA4 HeLa cells showed a greater uniformity in the Ca^{2+} transients compared to the control cells (see also movie S1). The $[Ca^{2+}]_i$ in a subpopulation of control HeLa cells returned to baseline faster than in the other cells, indicating substantial variability in the extrusion capacity between cells. Because this subpopulation was absent in the sh-PMCA4 cells, differences in PMCA4 abundance in individual control cells may contribute to this variability. These experiments suggested that PMCA4 plays an important role in Ca^{2+} clearance during SOCE-induced Ca^{2+} transients, consistent with previous findings *(24, 27, 31, 32)*.

Slow PMCAs generate an oscillating Ca^{2+} response following SOCE

On the basis of their distinct activation and inactivation kinetics, PMCAs are categorized into slow and fast pumps, and pumps with a short or long "memory" of previous activation. To examine the influence of PMCAs in these different categories on the SOCE-mediated Ca^{2+} signal, we created mCherry-tagged PMCA constructs: mCherry-PMCA4b (slow with memory), mCherry-PMCA4a (fast with short memory), and mCherry-PMCA2b (fast with long memory). We have shown previously *(33)* that the plasma membrane delivery of PMCA4b was most efficient in confluent cells and that three consecutive leucine residues ($Leu^{1167-1169}$) at the C-terminal region were responsible for its enhanced internalization under subconfluent conditions. Therefore, in certain experiments we used the PMCA4b-LA mutant in which these leucines were replaced by alanines, resulting in enhanced plasma membrane localization of PMCA4b without affecting PMCA4b activity *(33)*. We used the mCherry signal to identify the PMCA-transfected cells, enabling analysis of the SOCE-mediated Ca^{2+} signal and PMCA abundance simultaneously at the single-cell level. To allow direct comparison of the experimental data, we selected cells

with similar abundance of the PMCAs (mCherry intensity), analyzed confluent cultures, and acquired the data with identical acquisition parameters and settings.

We analyzed the effect of the slow PMCA4b pump on SOCE-mediated Ca^{2+} transients in HeLa cells transiently transfected with GCaMP2 and mCherry-PMCA4b or mCherry-PMCA4b-LA. Compared with the Ca^{2+} transients in control HeLa cells (Fig. 1C) or the sh-PMCA4 cells (Fig. 1D), the cells with either mCherry-PMCA4b or mCherry-PMCA4b-LA had a different pattern of Ca^{2+} transient (Fig. 2A, B): Following the first peak in $[Ca^{2+}]_i$, Ca^{2+} returned much faster to the baseline concentration in the either mCherry-PMCA4b or mCherry-PMCA4b-LA cells. Additionally, in many of the mCherry-PMCA4b or mCherry-PMCA4b-LA cells, we observed periodic baseline oscillations (Fig. 2A and B). The pattern of Ca^{2+} transients was more variable among different cells expressing mCherry-PMCA4b (Fig. 2A) compared with the highly synchronized oscillations in the mCherry-PMCA4b-LA-expressing cells (Fig. 2B, movie S2), which may be due to a more uniform plasma membrane localization of the mutant. The number of Ca^{2+} peaks during a 10-minute recording period was ~3-4 in mCherry-PMCA4b-LA cells and was 2-3 peaks in the mCherry-PMCA4b cells. We confirmed the presence of the mCherry-tagged proteins by Western blotting, which showed that these proteins were produced in excess of the endogenous proteins (Fig. 2C).

Previous experiments suggested that PMCAs were primarily responsible for removing Ca^{2+} after a moderate SOCE-mediated spike and for determining resting $[Ca^{2+}]_i$ in endothelial cells *(26)*;*(34)*. We found that primary endothelial cells isolated from human umbilical veins (HUVECs) had a greater abundance of PMCA4b than PMCA1b (Fig. 2C) and that PMCA2 or PMCA4a were not detectable. We analyzed the SOCE-mediated Ca^{2+} signal in HUVECs loaded with the Ca^{2+} indicator dye Fluo4. Because our previous studies suggested that the PMCA4b protein was in the plasma membrane only in confluent HUVEC cultures *(33)*, we analyzed Ca^{2+}

signals using the Ca^{2+} re-addition method in confluent cultures. SOCE induced an initial peak that was followed by a few irregular Ca^{2+} spikes (Fig. 2D), similar to the pattern seen in the mCherry-PMCA4b-overexpressing HeLa cells (Fig. 2A, B). Application of the SOCE channel inhibitor BTP2 abolished Ca^{2+} entry (Fig. 2E), confirming that Ca^{2+} signal arose from SOCE, which is consistent with previous findings *(35)*.

Fast PMCAs with long or short memory generate distinct Ca^{2+} responses following SOCE

We transiently expressed the fast with a short memory PMCA4a (tagged with mCherry) and the fast with a long memory PMCA2b (tagged with mCherry) along with GCaMP2 in the sh-PMCA4 cells to evaluate if these different classes of PMCAs produced distinct patterns of Ca^{2+} signal in response to SOCE. Cells expressing mCherry-PMCA4a exhibited a quick rise in Ca^{2+} that was followed by a rapid decline to a new, elevated $[Ca^{2+}]i$ (Fig. 2F). In contrast, cells expressing mCherry-PMCA2b rapidly cleared the Ca^{2+}, returning $[Ca^{2+}]_i$ to baseline in less than 30 s (Fig. 2G).

The patterns of Ca^{2+} transients induced by various stimuli are governed by the kinetic properties of the PMCA isoforms

To determine if PMCA isoforms also influenced the patterns of Ca^{2+} signals produced in response to a SOCE-independent increase in $[Ca^{2+}]i$, we used the calcium ionophore A23187 in the presence of 2 mM external calcium to promote a cytosolic calcium signal independent from the plasma membrane channels in HeLa cells. Surprisingly, the patterns of Ca^{2+} signals were quite similar to those triggered by SOCE in the presence of the various PMCAs (fig. S1). Control HeLa cells produced variable responses (fig. S1A), similar to those produced by SOCE (Fig. 1C). Cells expressing mCherry-PMCA4b-LA exhibited an oscillating pattern under both stimulation conditions (fig. S1B, Fig. 2B). Expression of mCherry-PMCA2b resulted in rapid clearance and

Ca^{2+} declined to basal concentrations (fig. S1C, Fig. 2G), and expression of mCherry-PMCA4a resulted in an increased [Ca^{2+}]i, following the initial spike (fig. S1C, Fig. 2F).

Human embryonic kidney 293 (HEK293) cells are a widely used and easily transfected cell line. Therefore, we tested if the distinct pattern produced by the different PMCAs in HeLa cells was also generated in these cells. First, we determined by Western blotting that, although PMCA1 is the main isoform in both HeLa and HEK293 cells, the abundance of PMCA1 is greater in HEK293 cells than in HeLa cells (fig. S2A). Despite the relatively high abundance of PMCA1 in HEK293 cells, the SOCE-mediated signal changed dramatically when PMCAs were overexpressed in HEK293 cells, replacing the pattern seen in the control cells (fig. S2B-E) and suggesting that the kinetic property of the most abundant PMCA isoform determines the shape of the Ca^{2+} signal.

The SOCE-induced Ca^{2+} transient is sensitive to the abundance of PMCA2b but less sensitive to the abundance of the PMCA4 variants

To determine if the Ca^{2+} signal depended on the abundance of the PMCA isoform, we generated a HeLa cell line stably expressing GCaMP2 using the Sleeping-Beauty transposon expression system. This cell line provided uniform expression of the GCaMP2 sensor, enabling testing of the SOCE-meditated signal in cells expressing various amounts of PMCA by transient transfection of the cells with the appropriate mCherry-PMCA constructs. We quantified the peak areas of the Ca^{2+} signal from the Ca^{2+} transients (GCaMP2 signal) in individual cells and plotted those data against the mCherry-PMCA abundance determined from the relative fluorescence intensities of individual cells. Fluorescence intensity acquired in each confocal image was taken at the same acquisition parameters and settings for all mCherry-PMCA constructs. The influence of the abundance of mCherry-PMCA4b or mCherry-PMCA4a on the Ca^{2+} signal was relatively modest (Fig. 3A and B). In contrast, calcium handling in mCherry-PMCA2b-expressing cells was

highly sensitive to small alterations in the abundance of PMCA2b: The Ca^{2+} peak area dropped exponentially as mCherry-PMCA2b abundance increased (Fig. 3C and D). Further, the resting $[Ca^{2+}]_i$ was independent of the presence of the mCherry-PMCAs (Fig. 3E and F), indicating that the characteristic changes in the Ca^{2+} signal were not due to differences in the resting $[Ca^{2+}]_i$.

SOCE is responsible for the sustained Ca^{2+} entry

To confirm that the Ca^{2+} entry was mediated by the SOCE channels, we tested the effects of the inhibitors SKF-96365 and BTP2 *(36)*. We monitored Ca^{2+} signals in HeLa cells expressing mCherry-PMCA4a or mCherry-PMCA4b-LA but added SKF-96365 ten minutes after SOCE initiation (Fig. 4A, B) or BTP2 before SOCE initiation (Fig. 4C, D). The SOCE-induced Ca^{2+} signals were terminated and $[Ca^{2+}]_i$ returned quickly to baseline after SKF-96365 addition in both the mCherry-PMCA4a-expressing or mCherry-PMCA4b-LA-expressing cells. BTP2 completely blocked the Ca^{2+} signal in the mCherry-PMCA4a-expressing cells (Fig. 4C) and eliminated the oscillations in the mCherry-PCMA4b-LA-expressing cells (Fig. 4D). These experiments suggest that the oscillations or sustained increase in $[Ca^{2+}]_i$ resulted from an interplay between the activity of the SOCE channels and the PMCAs.

The PMCA-controlled SOCE pattern is retained at different extracellular Ca^{2+} concentrations

Because Ca^{2+} entry through SOCE channels and its inhibition by Ca^{2+}-calmodulin depends on the extracellular concentration of Ca^{2+} ($[Ca^{2+}]_e$) *(37)*, we tested how changing $[Ca^{2+}]_e$ affected the SOCE-induced Ca^{2+} pattern in the presence of the different PMCAs (Fig. 5). To initiate SOCE following store depletion with thapsigargin, $[Ca^{2+}]$ of the incubation medium was increased by a stepwise addition of 0.5, 1, and 2 mM Ca^{2+}, and Ca^{2+} signals were monitored for 5 minutes after each addition. In sh-PMCA4 cells each increase in $[Ca^{2+}]_e$ resulted in an incremental increase in $[Ca^{2+}]_i$ (Fig. 5A). In contrast, cells expressing the fast-activating, short memory mCherry-

PMCA4a exhibited a return of $[Ca^{2+}]_i$ to the same elevated baseline induced following the first increase in $[Ca^{2+}]_e$ (Fig. 5B). Interestingly, the spike induced by 0.5 mM $[Ca^{2+}]_e$ was the largest, suggesting that at the elevated baseline $[Ca^{2+}]_i$ PMCA4a could respond more rapidly to the next increase in Ca^{2+}, resulting in smaller peaks after the second and third additions of $[Ca^{2+}]_e$. Cells expressing the fast-activating, long memory mCherry-PMCA2b produced a smaller initial Ca^{2+} transient than either the sh-PMCA4 or mCherry-PMCA4a-expressing cells and the change in $[Ca^{2+}]_i$ following the exposure to 1 mM and 2 mM $[Ca^{2+}]_e$ was negligible (Fig. 5C). Cells expressing mCherry-PMCA4b-LA, which is the slow with memory isoform, exhibited equally large spikes after each addition (Fig. 5D). This indicated that PMCA2b remained mostly activated during the experiment; whereas PMCA4b became inactivated after each Ca^{2+} challenge by the end of the 5-minute incubation period. Thus, these experiments indicated that PMCAs with different memory properties and activation kinetics contribute to the character of the SOCE-mediated Ca^{2+} signal even at distinct $[Ca^{2+}]_e$.

Modeling of the SOCE-mediated Ca^{2+} signal supports the essential role of different PMCA isoforms in shaping the signal

We generated a simplified kinetic model that accounts for steps including Ca^{2+} entry through the SOCE channel and Ca^{2+} extrusion from the cell through the PMCA (Table 2, chemical equations; text S1, differential equations). The model is based on a previously designed system *(15)* except that here Ca^{2+} handling through the ER Ca^{2+} pool is not considered (because our experimental system eliminated ER Ca^{2+} participation by the use of thapsigargin and pool depletion) and the representation of SOCE is updated. SOCE is indicated in equations (1-3) where equation (1) represents clustering of the channel molecules (STIM and ORAI); equation (2) represents Ca^{2+} entry through the channel; and equation (3) describes inhibition of the channel by Ca^{2+}-CaM binding *(37)*. Equations 4 through 12 describe reactions of PMCA-mediated Ca^{2+}

expulsion *(15)*. The equations (4-5) and (9-10) represent the basal and the Ca^{2+}-CaM-activated PMCA activity, respectively *(38, 39)*. The formation of the Ca^{2+}-CaM complex is described in equations (6) and (7). We could not obtain satisfactory fits of the PMCA4b data by the model unless we included 2 classes of sites for Ca^{2+} in CaM. Therefore, cooperative binding of Ca^{2+} to CaM was one property necessary to achieve oscillations. Equations (8) and (11-12) represent the association of the pump with and dissociation of the pump from Ca^{2+}-CaM. Ca^{2+}-CaM targets other than the SOC channel and PMCA, are summarized as T. The introduction of other Ca^{2+}-CaM targets was important to provide some buffering for free Ca^{2+}-CaM.

Because the rate constants for PMCA4b have already been published *(15)* (Table 3), we used the published parameters and fitted the data obtained from cells expressing mCherry-PMCA4b (Fig. 6A, B). Fitting the data from mCherry-PMCA2b-expressing and mCherry-PMCA4a-expressing cells while using the parameters previously obtained from modeling the PMCA4b data [except the protein concentrations and the kinetic parameters of PMCA2b and 4a *(15, 17, 19)*; see Table 3] failed. Therefore, we only fixed the previously determined kinetic parameters of the PMCA isoforms *(15, 19)* and through fitting found the sets of parameters that yielded best fit curves within the error bars of experimental data. From these parameter sets, we chose the ones in which the parameters not directly related to PMCA were within an order of magnitude of the same parameters obtained for the PMCA4b fit (Table 3) and used them as starting points for further fitting. Eventually with this approach, we determined parameters that effectively reproduced the data (Fig. 6C, D), thereby providing mathematical support that the unique shape of each curve can be attributed to the different kinetic and regulatory characteristics of the PMCA isoforms.

We used the model to explore how the properties of the system produced Ca^{2+} oscillations. We performed simulations of the change in $[Ca^{2+}]_i$ over time using the parameters obtained by

data fitting (Table 3) and the DynaFit software (www.biokin.com). Of the 3 PMCA variants tested, only the slow PMCA4b produced sustained oscillations (Fig. 2A, B) and the simulations showed that the slow activation of PMCA4b is important for generating the Ca^{2+} waves (Fig. 7). Simulations that produced Ca^{2+} oscillations like those observed in the PMCA4b-expressing cells indicated a temporal shift between the activation of the SOCE channel and the pump (Fig. 7A, B): The channel is predicted to become quickly activated followed by slower activation of the PMCA4b pump. After the first peak in activity, both the channel and pump activities are predicted to return to baseline (Fig. 7A). The simulations revealed a similar pattern of the activities of both pump and channel during the Ca^{2+} oscillatory phase, although at a smaller scale (Fig. 7B).

We repeated the simulations varying the rate constant for Ca^{2+}-CaM association to PMCA (k_8) or dissociation from PMCA (k'_8) (Fig. 7C, D). In the simulations, k_8=0.2 $s^{-1}\mu M^{-1}$ and k'_8=0.0008 s^{-1} represent curves with the kinetic values of PMCA4b (*thick blue curve*). These simulations revealed the importance of k_8 in determining the presence of oscillations. The oscillatory pattern persisted when the value for k_8 was below 0.2 (k_8<0.2 $s^{-1}\mu M^{-1}$), imitating a super slow pump; the only difference was that the Ca^{2+} peaks became steeper and were shifted to the right. In contrast, when k_8 was set to higher values (k_8>0.2 $s^{-1}\mu M^{-1}$), representing a faster activating pump like PMCA2b, the oscillation dampened (Fig. 7D). Varying k'_8 did not diminish the oscillations (Fig. 7E), indicating that the Ca^{2+} oscillations primarily required the slow activation of PMCA by Ca^{2+}-CaM. The simulations indicated that slow binding allows Ca^{2+} to build up before PMCA is fully activated, such that Ca^{2+} entry peaks and Ca^{2+} extrusion become out of phase.

Because our experiments suggested that the amount of pump present in the membrane was an important determine of Ca^{2+} oscillations, we explored this property with the model as well. We

found that varying the concentration of the pump in the simulations affected both the first peak and secondary spikes (Fig. 7F) in a manner similar to that determined experimentally (Figs. 2A and 3A).

Discussion

Previous studies documented that the PMCA is an essential component of SOCE-mediated Ca^{2+} signaling in non-excitable cells *(26, 28, 40)*. In addition to its basic function as a global calcium efflux system, PMCAs can regulate IP_3-mediated intracellular Ca^{2+} signaling by controlling the amount of phosphatidylinositol-4,5-bisphosphate in the plasma membrane, a function of these proteins that is at least partly independent of calcium-pumping activity *(29)*. Here, we investigated how PMCA isoforms with different kinetic parameters changed the pattern of the SOCE-mediated Ca^{2+} signal and found that both activation and inactivation kinetics determined by the kinetics of the interaction between Ca^{2+}-CaM and the specific PMCA played a role. We found that different shapes of Ca^{2+} signals (oscillation or discrete peaks) were characterized by the presence of fast or slow PMCA pumps.

We then used our data to create a mathematical model of the contribution of PMCAs to shaping SOCE-induced Ca^{2+} transients, which confirmed that slow activation of PMCA4b due to its slow association with Ca^{2+}-CaM was critical to producing oscillating Ca^{2+} signals. The rate constant determined by model fitting for the inactivation of the store-operated channel by Ca^{2+}-CaM is relatively high ($k_3 \sim 2.5\ s^{-1}\mu M^{-1}$), which would result in fast channel inactivation consistent with previous findings *(37, 41)*. Thus, it is possible that the rhythm of the Ca^{2+} waves is controlled by the PMCA rather than by the SOCE channels *(41)*. In agreement with this notion, artificially triggered Ca^{2+} entry by A23187 (fig. S1) mimicked the PMCA-mediated Ca^{2+} signal

patterns. However, in cells under normal stimulating conditions, both SOCE and PMCA likely contribute to the pattern of the Ca^{2+} signal.

Because the slow activation of PMCA4b is a direct consequence of slow binding and the "conformational collapse" of CaM *(42, 43)*, our model highlights the role of CaM in several aspects of the Ca^{2+} signal. Ca^{2+}-CaM regulates not only the PMCA but also Ca^{2+} entry through the STIM-ORAI channels. Our model predicts that SOCE is inhibited by Ca^{2+}-CaM and can close without store refilling in agreement with data obtained in HEK, HeLa, and human umbilical vein endothelial cells *(37, 44, 45)*. Our findings also agree with those of Bird *et al*. *(46)* who showed transient activation of STIM1 during methacholin-induced Ca^{2+} oscillation in HEK293 cells.

The regulation and complexity of Ca^{2+} oscillation have long been a challenge in the Ca^{2+}-signaling field and multiple modeling approaches have been applied to understand its mechanisms *(47-49)*. Most computational models, however, use a plasma membrane Ca^{2+} channel and uptake of Ca^{2+} into and release of Ca^{2+} from the ER to sustain Ca^{2+} oscillations. These models incorporate PMCA as a simple Ca^{2+}-efflux mechanism and use parameters allowing the best fit in the particular experimental and computational set-up. Here, by keeping the ER store empty, we could observe and model oscillations established by a slow PMCA and a Ca^{2+}-entry channel. In addition to the data presented here, we know of only one other study in undifferentiated human bone marrow-derived mesenchymal stem cells that suggested that both Ca^{2+} entry through plasma membrane channels and Ca^{2+} extrusion mediated by PMCAs and NCXs were crucially important in generating sustained Ca^{2+} oscillations *(50)*.

The fast pumps generated a very different pattern of the Ca^{2+} signal from that of the slow PMCA4b. Among the fast pumps, PMCA2b has a long memory; whereas PMCA4a has a short memory *(18, 19)*. Short memory indicates that CaM dissociates rapidly from the pump; therefore, the pump is inactivated quickly after the first Ca^{2+} spike. In a cell, the fast pumps will respond

quickly to the incoming Ca^{2+} signal. However, as the $[Ca^{2+}]_i$ drops, PMCA4a becomes inactivated quickly because of its short memory, resulting in a relatively high steady-state $[Ca^{2+}]_i$ after the spike. The sustained increase in $[Ca^{2+}]_i$ requires constant Ca^{2+} influx, because $[Ca^{2+}]_i$ will otherwise return to the baseline soon after SOCE is blocked (Fig. 4A). This short memory property of PMCA4a *(15, 19)* means that a cell with PMCA4a can respond to repeated stimuli (Fig. 5B). In contrast, PMCA2b - because of its long-lasting memory and a relatively high basal activity - stays active after $[Ca^{2+}]_i$ declines and therefore depresses any additional incoming signal, even if the SOCE channel or other Ca^{2+} channels remain active after the spike. Thus, presence of the PMCA2b isoform allows discrete Ca^{2+} spikes - like the ones seen in cerebellar Purkinje neurons *(51, 52)* - but will restore $[Ca^{2+}]_i$ to its low basal level despite the large demand on extrusion generated by the opening of the Ca^{2+} channels.

The physiological situation is more complex than our simple model predicts. For example, in our model we assume one generic Ca^{2+}-CaM target. In cells, there are hundreds of CaM targets, each with its own affinity for CaM and Ca^{2+}. Indeed, the free CaM concentration may be limited depending on cell type and the relative abundance of the different CaM targets and CaM *(53)*. Similarly, the cytosol contains several proteins that act as Ca^{2+} buffers but these were not included in our model nor were the effects of mitochondria. Although these factors are important in cells, they were not necessary to fit the model to the data accurately.

The delayed activation of PMCA4b is a determining factor in shaping the SOCE response in endothelial cells *(26, 28)* and the tuning of the Ca^{2+} signal in T cell activation *(24, 40)*. A physical interaction between STIM1 and PMCA4 occurs at the region of the immunological synapse, and this interaction inhibits PMCA-mediated Ca^{2+} clearance *(27)*. Furthermore, STIM1, ORAI1, and POST (partner of STIM1) interact with and inhibit PMCA upon store depletion *(54-56)*.

In conclusion, using HeLa and HEK293 cells, as well as primary endothelial cells, we showed that PMCA isoforms differentially affected the outcome of SOCE-induced signals. The slow PMCA4b sustained Ca^{2+} oscillations in the absence of store refilling; whereas the fast PMCA2b with its long-lasting memory efficiently cleared SOCE-induced Ca^{2+} signals back to baseline. PMCA4a, a fast pump with short memory, reduced SOCE-induced Ca^{2+} but produced a sustained elevation above baseline in $[Ca^{2+}]_i$ without oscillations. The shape and kinetics of the SOCE-induced Ca^{2+} responses were adequately described by a mathematical model that takes into account the Ca^{2+}-CaM binding and activation kinetics of the PMCA isoforms. Our results provide evidence for the involvement of different PMCAs in shaping distinct Ca^{2+} responses.

Materials and methods

Reagents and antibodies.

Pan-PMCA specific monoclonal mouse antibody 5F10, human PMCA4b-specific monoclonal mouse antibody JA3, and rabbit polyclonal antibody recognizing PMCA2 (NR2), have been described *(57)*. A rabbit polyclonal antibody recognizing PMCA1 was obtained from Affinity BioReagents and a mouse monoclonal antibody recognizing Na,K-ATPase (α3 subunit) was from Enzo Life Sciences. Fugene HD Transfection Reagent was obtained from Roche Applied Science (Mannheim, Germany). All other chemicals used were of reagent grade.

DNA constructs.

pN1-GCaMP2 plasmid was a kind gift of Junichi Nakai, RIKEN Brain Science Institute, Saitama, Japan *(58)*. Generation of the mCherry-PMCA4b construct *(33)* and the mCherry-PMCA4b-L1167-1169A mutant construct *(29)* were described previously. mCherry-PMCA4a was made by replacing the 1.2 kb *Eco*RI fragment of mCherry-PMCA4b encoding the C terminus of PMCA4b with the corresponding 1.4 kb *Eco*RI fragment from pMM2-PMCA4a *(17)*. The

mCherry-PMCA2b construct was created by replacing the EGFP fragment of pEGFP-C1-PMCA2x/b *(59)* with the mCherry coding sequence from the pmCherry-C1 vector (Clontech) using the *Age*I-*Kpn*I restriction sites.

Cell culture and transfection.

HeLa and HEK293 cells were grown in DMEM supplemented with 10% FBS, 100 U/ml penicillin, 100 μg/ml streptomycin, and 2 mM glutamine under 5% CO_2 at 37^{o}C. One day prior to transfection cells were seeded into a Lab-Tek^{TM} II Chambered Slide (Nalge Nunc Int.) at 4-6x10^{4} cell density. Transfection was performed with FuGene HD (Roche) according to the protocol of the manufacturer. This procedure yielded about 70-80% transfected cells. Cells were analyzed 48 hours after transfection. The sh-PMCA4 HeLa cell line was generated by transfecting HeLa cells with a PMCA4 shRNA plasmid (Santa Cruz Biotechnology, Inc.) as described *(29)*. HUVEC cells were freshly isolated from human umbilical cord veins by the Institute of Pathophysiology (Semmelweis University, Budapest, Hungary) as described in *(60, 61)*. Cells from passages 2–4 were used for experiments.

Generation of stable GCaMP2-expressing HeLa cell lines using the Sleeping Beauty (SB) transposon system.

A DNA fragment encoding GCaMP2 was PCR-generated with *Age*I(5')/*Bgl*II(3') restriction sites at its ends. Primer sequences were as follows: forward, 5'-CTACCGGTCTCGCCACCAATG-3'; and reverse, 5'-AGATCTCCGCTCACTTCGCTGTC-3'. The complete GCaMP2 DNA-fragment was put into an SB-CAG-Amaxa GFP vector from which Amaxa GFP was excised with *Age*I and *Bgl*II enzymes. The GCaMP2 fragment in the resulting vector is flanked on both sides by an inverted repeat-direct repeat (IRDR) region, which is the recognition motif of *Sleeping Beauty* (SB) transposase *(62, 63)*, and the construct also contains a CAG promoter. Cells were cotransfected with a SB transposase plasmid and the SB-CAG-

GCaMP2 transposon plasmid in a 10:1 ratio using FuGENE® HD reagent. An enhanced version of the transposase was used that has an approximately hundred-fold higher activity than the original transposase *(64)*. Following transfection, cells were cultured for 2 weeks, trypsinized, and single cell clones were generated by dilution into 96-well plates. Individual GCaMP2-expressing clones were identified by GFP fluorescence using a fluorescent microscope and expanded. HeLa-GCaMP2 clones were used in the experiments described in Figure 3.

SOCE measurements using the 'Ca^{2+}-re-addition' protocol.

Cells were seeded into a Lab-Tek™ II Chambered Slide (Nalge Nunc Int.). HeLa and HEK293 cells were transfected with the appropriate constructs using FuGENE® HD reagent as described above. Before confocal imaging, cells were switched to Phenol Red-free DMEM supplemented with 10% FBS, 10 mM HEPES (pH 7.4) and incubated for two hours. HUVECs were loaded with 1 μM Fluo4/AM at room temperature for 30 min. SOCE was measured according to the "Ca^{2+} re-addition" protocol with some modifications *(65)*. In all cases, prior to Ca^{2+}-store depletion the culture medium was replaced with nominally Ca^{2+}-free Hank's Buffered Salt Solution (HBSS) supplemented with 0.9 mM $MgCl_2$, 100 μM EGTA, 100 μM $CaCl_2$, and 20 mM Tris (pH 7.6; ~2μM free Ca^{2+}). SOCE channels are inhibited under acidic conditions; therefore, extracellular pH 7.6 was applied to ensure high SOCE channel activity *(66)*. Intracellular Ca^{2+} stores were depleted by the addition of 2 μM thapsigargin (Tg) combined with 100 μM ATP or 500 nM ionomycin to reach full store depletion in a relatively short period of time (5 minutes). The combined treatment was necessary to avoid long incubation of cells in the Ca^{2+}-free media that may damage cell-cell junctions and result in cell detachment from cell culture surfaces *(67, 68)*. SOCE was initiated by the re-addition of $CaCl_2$ to adjust external Ca^{2+} concentration to 2 mM. Optionally, 50 μM SKF-96365 or 10 μM BTP2 was added, as indicated. Images were taken with an Olympus IX-81 laser scanning confocal microscope and Fluoview

FV500 (v4.1) software using an Olympus PLAPO 60× (1.4) oil immersion objective. For GCaMP2 and Fluo4 imaging, cells were excited at 488 nm and emission was collected between 505 and 535 nm. mCherry-tagged PMCAs were illuminated at 543 nm and emission above 560 nm was recorded. Images were acquired every 0.3 s, z-resolution was 1 μm. Time- lapse sequences were recorded with Fluoview Tiempo (v4.3) time course software at room temperature. The relative fluorescence was calculated as F/F_0 (where F_0 was the average initial fluorescence). GraphPad Prism4 software (http://www.graphpad.com) was used to analyze the experimental data. Images were processed with ImageJ and Prism Video File Converter Plus (v1.82) was used to generate QuickTime videos. Maximum (F_{max}) and minimum (F_{min}) GCaMP2 fluorescence were determined at the end of the experiments by the addition of 5 μM ionomycin and 10 mM EGTA, respectively. In some cases 0.1% DOC (deoxycholate) was also added to permeabilize the cells. $[Ca^{2+}]_i$ in control and transfected HeLa-GCaMP2 cells was determined by using the K_d value and Hill coefficient described previously *(69)*.

Electrophoresis and Western blotting.

HeLa and HEK293 cells were transfected with the appropriate constructs as above. Two days after transfection, cells were precipitated with ice-cold 6% trichloroacetic acid and resuspended in an electrophoresis sample buffer containing 62.5 mM Tris-HCl, pH 6.8, 2% SDS, 10% glycerol, 5 mM EDTA, 100 mM dithiothreitol and 125 mg/ml urea. If necessary, samples were neutralized by 1.7 M Tris, pH 8.8. Proteins in these cell lysates were separated by SDS-PAGE on 7.5% acrylamide gels and were subsequently electroblotted onto PVDF membranes (Bio-Rad) and immunostained by antibodies recognizing all isoforms of PMCA [5F10 (1:5000)], PMCA4b [JA3 (1:1000)], PMCA1 (1:500), PMCA2 [NR2 (1:500)] or Na^+,K^+-ATPase (1:2000). Secondary antibody [anti-mouse-HRP or anti-rabbit-HRP (Jackson ImmunoResearch)] binding was detected by the ECL detection kit (Amersham).

Data fitting.

To fit the data by model equations, we employed a weighted nonlinear least-squares method. The initial attempts of fitting with DynaFit software (www.biokin.com) did not yield satisfactory results. Therefore, we used custom-made software based on Simplex Induction Hybrid algorithm for minimization, which compares favorably with other algorithms for challenging optimization problems *(70)*. Our software can limit parameter values within prescribed boundaries and includes many starting points that are generated automatically. The system of differential equations was solved by the fast and reliable LSODA numerical solver, which automatically uses appropriate methods for stiff and non-stiff equations (www.oecd-nea.org/tools/abstract/detail/uscd1227) that may alternate as a result of changing the rates during minimization. The weights for least-squares fitting were standard: inverse variances estimated from multiple measurements.

To relate the fluorescence ratios generated by the GCaMP2 indicator to cytosolic Ca^{2+} concentrations, we determined F_{max} and F_{min} as described above and used the Hill equation with the parameters given by Willoughby *et al*. *(69)*. Differential equations are included as text S1.

The simulations performed (Fig. 7) were obtained with DynaFit, which was adequate for that task and more user friendly than our custom-made software.

Supplementary Materials

Text S1. *The system of rate equations describing the kinetic model.*

Figure S1. *A23187-induced Ca^{2+} signaling of control HeLa cells or HeLa cells expressing mCherry-PMCA4b-LA, mCherry-PMCA4a or mCherry-PMCA2b.*

Figure S2. *HEK293 cells generate the typical shape of the Ca^{2+} signals of the slow and fast PMCAs.*

Movie S1. *SOCE signal in sh-PMCA4 HeLa cells*.

Movie S2. *SOCE-mediated transients in HeLa cells cotransfected with mCh-PMCA4b-LA and GCaMP2*.

References

1. R. S. Lewis, The molecular choreography of a store-operated calcium channel. *Nature* **446**, 284-287 (2007).
2. J. T. Smyth, S. Y. Hwang, T. Tomita, W. I. DeHaven, J. C. Mercer, J. W. Putney, Activation and regulation of store-operated calcium entry. *J Cell Mol Med* **14**, 2337-2349 (2010).
3. S. Feske, E. Y. Skolnik, M. Prakriya, Ion channels and transporters in lymphocyte function and immunity. *Nat Rev Immunol* **12**, 532-547 (2012).
4. W. C. Chang, C. Nelson, A. B. Parekh, Ca2+ influx through CRAC channels activates cytosolic phospholipase A(2), leukotriene C-4 secretion, and expression of c-fos through ERK-dependent and -independent pathways in mast cells. *Faseb J* **20**, 2381-2383 (2006).
5. D. M. F. Cooper, M. Yoshimura, Y. X. Zhang, M. Chiono, R. Mahey, Capacitative Ca2+ Entry Regulates Ca2+-Sensitive Adenylyl Cyclases. *Biochem J* **297**, 437-440 (1994).
6. J. Di Capite, A. B. Parekh, CRAC channels and Ca2+ signaling in mast cells. *Immunol Rev* **231**, 45-58 (2009).

7. S. W. Ng, C. Nelson, A. B. Parekh, Coupling of Ca2+ Microdomains to Spatially and Temporally Distinct Cellular Responses by the Tyrosine Kinase Syk. *J Biol Chem* **284**, 24767-24772 (2009).

8. J. W. Putney, The Physiological Function of Store-operated Calcium Entry. *Neurochem Res* **36**, 1157-1165 (2011).

9. S. Feske, Immunodeficiency due to defects in store-operated calcium entry. *Year in Human and Medical Genetics: Inborn Errors of Immunity I* **1238**, 74-90 (2011).

10. M. Oh-hora, Calcium signaling in the development and function of T-lineage cells. *Immunol Rev* **231**, 210-224 (2009).

11. A. B. Parekh, J. W. Putney, Store-operated calcium channels. *Physiol Rev* **85**, 757-810 (2005).

12. M. J. Berridge, M. D. Bootman, H. L. Roderick, Calcium signalling: Dynamics, homeostasis and remodelling. *Nat Rev Mol Cell Bio* **4**, 517-529 (2003).

13. E. E. Strehler, A. J. Caride, A. G. Filoteo, Y. N. Xiong, J. T. Penniston, A. Enyedi, Plasma membrane Ca2+ ATPases as dynamic regulators of cellular calcium handling. *Ann Ny Acad Sci* **1099**, 226-236 (2007).

14. A. J. Caride, N. L. Elwess, A. K. Verma, A. G. Filoteo, A. Enyedi, Z. Bajzer, J. T. Penniston, The rate of activation by calmodulin of isoform 4 of the plasma membrane Ca2+ pump is slow and is changed by alternative splicing. *J Biol Chem* **274**, 35227-35232 (1999).

15. A. J. Caride, A. G. Filoteo, J. T. Penniston, E. E. Strehler, The plasma membrane Ca2+ pump isoform 4a differs from isoform 4b in the mechanism of calmodulin binding and activation kinetics - Implications for Ca2+ signaling. *J Biol Chem* **282**, 25640-25648 (2007).

16. N. L. Elwess, A. G. Filoteo, A. Enyedi, J. T. Penniston, Plasma membrane Ca2+ pump isoforms 2a and 2b are unusually responsive to calmodulin and Ca2+. *J Biol Chem* **272**, 17981-17986 (1997).

17. A. Enyedi, A. K. Verma, R. Heim, H. P. Adamo, A. G. Filoteo, E. E. Strehler, J. T. Penniston, The Ca2+ Affinity of the Plasma-Membrane Ca2+ Pump Is Controlled by Alternative Splicing. *J Biol Chem* **269**, 41-43 (1994).

18. A. J. Caride, A. G. Filoteo, A. R. Penheiter, K. Paszty, A. Enyedi, J. T. Penniston, Delayed activation of the plasma membrane calcium pump by a sudden increase in Ca2+: fast pumps reside in fast cells. *Cell Calcium* **30**, 49-57 (2001).

19. A. J. Caride, A. R. Penheiter, A. G. Filoteo, Z. Bajzer, A. Enyedi, J. T. Penniston, The plasma membrane calcium pump displays memory of past calcium spikes - Differences between isoforms 2b and 4b. *J Biol Chem* **276**, 39797-39804 (2001).

20. T. P. Stauffer, H. Hilfiker, E. Carafoli, E. E. Strehler, Quantitative analysis of alternative splicing options of human plasma membrane calcium pump genes. *The Journal of biological chemistry* **268**, 25993-26003 (1993).

21. E. E. Strehler, D. A. Zacharias, Role of alternative splicing in generating isoform diversity among plasma membrane calcium pumps. *Physiol Rev* **81**, 21-50 (2001).

22. M. Brini, L. Coletto, N. Pierobon, N. Kraev, D. Guerini, E. Carafoli, A comparative functional analysis of plasma membrane Ca2+pump isoforms in intact cells. *J Biol Chem* **278**, 24500-24508 (2003).

23. T. Domi, F. Di Leva, L. Fedrizzi, A. Rimessi, M. Brini, Functional specificity of PMCA isoforms? *Ann Ny Acad Sci* **1099**, 237-246 (2007).

24. D. M. Bautista, R. S. Lewis, Modulation of plasma membrane calcium-ATPase activity by local calcium microdomains near CRAC channels in human T cells. *J Physiol-London* **556**, 805-817 (2004).

25. A. Kamagate, A. Herchuelz, F. Van Eylen, Plasma membrane Ca(2+)-ATPase overexpression reduces Ca(2+) oscillations and increases insulin release induced by glucose in insulin-secreting BRIN-BD11 cells. *Diabetes* **51**, 2773-2788 (2002).

26. A. Klishin, M. Sedova, L. A. Blatter, Time-dependent modulation of capacitative Ca2+ entry signals by plasma membrane Ca2+ pump in endothelium. *Am J Physiol-Cell Ph* **274**, C1117-C1128 (1998).

27. M. F. Ritchie, E. Samakai, J. Soboloff, STIM1 is required for attenuation of PMCA-mediated Ca2+ clearance during T-cell activation. *Embo J* **31**, 1123-1133 (2012).

28. V. A. Snitsarev, C. W. Taylor, Overshooting cytosolic Ca2+ signals evoked by capacitative Ca2+ entry result from delayed stimulation of a plasma membrane Ca2+ pump. *Cell Calcium* **25**, 409-417 (1999).

29. J. T. Penniston, R. Padanyi, K. Paszty, K. Varga, L. Hegedus, A. Enyedi, Apart from its known function, the plasma membrane Ca2+ATPase can regulate Ca2+ signaling by controlling phosphatidylinositol 4,5-bisphosphate levels. *J Cell Sci* **127**, 72-84 (2014).

30. C. M. Ribeiro, R. R. McKay, E. Hosoki, G. S. Bird, J. W. Putney, Jr., Effects of elevated cytoplasmic calcium and protein kinase C on endoplasmic reticulum structure and function in HEK293 cells. *Cell Calcium* **27**, 175-185 (2000).

31. J. Chen, P. A. McLean, B. G. Neel, G. Okunade, G. E. Shull, H. H. Wortis, CD22 attenuates calcium signaling by potentiating plasma membrane calcium-ATPase activity. *Nat Immunol* **5**, 651-657 (2004).

32. A. Quintana, M. Pasche, C. Junker, D. Al-Ansary, H. Rieger, C. Kummerow, L. Nunez, C. Villalobos, P. Meraner, U. Becherer, J. Rettig, B. A. Niemeyer, M. Hoth, Calcium microdomains at the immunological synapse: how ORAI channels, mitochondria and calcium pumps generate local calcium signals for efficient T-cell activation. *The EMBO journal* **30**, 3895-3912 (2011).

33. G. Antalffy, K. Paszty, K. Varga, L. Hegedus, A. Enyedi, R. Padanyi, A C-terminal di-leucine motif controls plasma membrane expression of PMCA4b. *Biochim Biophys Acta* **1833**, 2561-2572 (2013).

34. H. S. Silva, A. Kapela, N. M. Tsoukias, A mathematical model of plasma membrane electrophysiology and calcium dynamics in vascular endothelial cells. *Am J Physiol Cell Physiol* **293**, C277-293 (2007).

35. I. F. Abdullaev, J. M. Bisaillon, M. Potier, J. C. Gonzalez, R. K. Motiani, M. Trebak, Stim1 and Orai1 mediate CRAC currents and store-operated calcium entry important for endothelial cell proliferation. *Circ Res* **103**, 1289-1299 (2008).

36. P. Varnai, L. Hunyady, T. Balla, STIM and Orai: the long-awaited constituents of store-operated calcium entry. *Trends Pharmacol Sci* **30**, 118-128 (2009).

37. F. M. Mullins, C. Y. Park, R. E. Dolmetsch, R. S. Lewis, STIM1 and calmodulin interact with Orai1 to induce Ca2+-dependent inactivation of CRAC channels. *P Natl Acad Sci USA* **106**, 15495-15500 (2009).

38. H. P. Adamo, A. F. Rega, P. J. Garrahan, Pre-Steady-State Phosphorylation of the Human Red-Cell Ca-2+-Atpase. *J Biol Chem* **263**, 17548-17554 (1988).

39. A. R. Penheiter, E. Bajzer, A. G. Filoteo, R. Thorogate, K. Torok, A. J. Caride, A model for the activation of plasma membrane calcium pump isoform 4b by calmodulin. *Biochemistry-Us* **42**, 12115-12124 (2003).

40. D. M. Bautista, M. Hoth, R. S. Lewis, Enhancement of calcium signalling dynamics and stability by delayed modulation of the plasma-membrane calcium-ATPase in human T cells. *J Physiol-London* **541**, 877-894 (2002).

41. A. Zweifach, R. S. Lewis, Rapid inactivation of depletion-activated calcium current (ICRAC) due to local calcium feedback. *J Gen Physiol* **105**, 209-226 (1995).

42. A. R. Penheiter, A. G. Filoteo, J. T. Penniston, A. J. Caride, Kinetic analysis of the calmodulin-binding region of the plasma membrane calcium pump isoform 4b. *Biochemistry-Us* **44**, 2009-2020 (2005).

43. J. T. Penniston, A. J. Caride, E. E. Strehler, Alternative Pathways for Association and Dissociation of the Calmodulin-binding Domain of Plasma Membrane Ca2+-ATPase Isoform 4b (PMCA4b). *J Biol Chem* **287**, 29664-29671 (2012).

44. R. Malli, S. Naghdi, C. Romanin, W. F. Graier, Cytosolic Ca(2+) prevents the subplasmalemmal clustering of STIM1: an intrinsic mechanism to avoid Ca(2+) overload. *J Cell Sci* **121**, 3133-3139 (2008).

45. W. W. Shen, M. Frieden, N. Demaurex, Local Cytosolic Ca2+ Elevations Are Required for Stromal Interaction Molecule 1 (STIM1) De-oligomerization and Termination of Store-operated Ca2+ Entry. *J Biol Chem* **286**, 36448-36459 (2011).

46. G. S. Bird, S. Y. Hwang, J. T. Smyth, M. Fukushima, R. R. Boyles, J. W. Putney, STIM1 Is a Calcium Sensor Specialized for Digital Signaling. *Curr Biol* **19**, 1724-1729 (2009).

47. S. Bandara, S. Malmersjo, T. Meyer, Regulators of calcium homeostasis identified by inference of kinetic model parameters from live single cells perturbed by siRNA. *Sci Signal* **6**, ra56 (2013).

48. G. Dupont, L. Combettes, G. S. Bird, J. W. Putney, Calcium Oscillations. *Csh Perspect Biol* **3**, (2011).

49. J. Sneyd, K. Tsaneva-Atanasova, D. I. Yule, J. L. Thompson, T. J. Shuttleworth, Control of calcium oscillations by membrane fluxes. *P Natl Acad Sci USA* **101**, 1392-1396 (2004).

50. S. Kawano, K. Otsu, S. Shoji, K. Yamagata, M. Hiraoka, Ca2+ oscillations regulated by Na+-Ca2+ exchanger and plasma membrane Ca2+ pump induce fluctuations of membrane currents and potentials in human mesenchymal stem cells. *Cell Calcium* **34**, 145-156 (2003).

51. R. M. Empson, M. L. Garside, T. Knopfel, Plasma membrane Ca2+ ATPase 2 contributes to short-term synapse plasticity at the parallel fiber to Purkinje neuron synapse. *J Neurosci* **27**, 3753-3758 (2007).

52. R. M. Empson, P. R. Turner, R. Y. Nagaraja, P. W. Beesley, T. Knopfel, Reduced expression of the Ca2+transporter protein PMCA2 slows Ca2+dynamics in mouse cerebellar Purkinje neurones and alters the precision of motor coordination. *J Physiol-London* **588**, 907-922 (2010).

53. N. Slavov, J. Carey, S. Linse, Calmodulin transduces Ca2+ oscillations into differential regulation of its target proteins. *ACS Chem Neurosci* **4**, 601-612 (2013).

54. T. R. Cully, J. N. Edwards, O. Friedrich, D. G. Stephenson, R. M. Murphy, B. S. Launikonis, Changes in plasma membrane Ca-ATPase and stromal interacting molecule 1 expression levels for Ca2+ signaling in dystrophic mdx mouse muscle. *Am J Physiol-Cell Ph* **303**, C567-C576 (2012).

55. G. Krapivinsky, L. Krapivinsky, S. C. Stotz, Y. Manasian, D. E. Clapham, POST, partner of stromal interaction molecule 1 (STIM1), targets STIM1 to multiple transporters. *P Natl Acad Sci USA* **108**, 19234-19239 (2011).

56. L. Vaca, SOCIC: The store-operated calcium influx complex. *Cell Calcium* **47**, 199-209 (2010).

57. A. J. Caride, A. G. Filoteo, A. Enyedi, A. K. Verma, J. T. Penniston, Detection of isoform 4 of the plasma membrane calcium pump in human tissues by using isoform-specific monoclonal antibodies. *Biochem J* **316**, 353-359 (1996).

58. J. Nakai, M. Ohkura, K. Imoto, A high signal-to-noise Ca2+ probe composed of a single green fluorescent protein. *Nat Biotechnol* **19**, 137-141 (2001).

59. M. C. Chicka, E. E. Strehler, Alternative splicing of the first intracellular loop of plasma membrane Ca2+-ATPase isoform 2 alters its membrane targeting. *J Biol Chem* **278**, 18464-18470 (2003).

60. C. Bodor, J. P. Nagy, B. Vegh, A. Nemeth, A. Jenei, S. MirzaHosseini, A. Sebe, L. Rosivall, Angiotensin II increases the permeability and PV-1 expression of endothelial cells. *Am J Physiol Cell Physiol* **302**, C267-276 (2012).

61. E. A. Jaffe, R. L. Nachman, C. G. Becker, C. R. Minick, Culture of human endothelial cells derived from umbilical veins. Identification by morphologic and immunologic criteria. *J Clin Invest* **52**, 2745-2756 (1973).

62. Z. Ivics, P. B. Hackett, R. H. Plasterk, Z. Izsvak, Molecular reconstruction of Sleeping beauty, a Tc1-like transposon from fish, and its transposition in human cells. *Cell* **91**, 501-510 (1997).

63. Z. Ivics, Z. Izsvak, Transposons for gene therapy! *Curr Gene Ther* **6**, 593-607 (2006).

64. L. Mates, M. K. L. Chuah, E. Belay, B. Jerchow, N. Manoj, A. Acosta-Sanchez, D. P. Grzela, A. Schmitt, K. Becker, J. Matrai, L. Ma, E. Samara-Kuko, C. Gysemans, D. Pryputniewicz, C. Miskey, B. Fletcher, T. VandenDriessche, Z. Ivics, Z. Izsvak, Molecular evolution of a novel hyperactive Sleeping Beauty transposase enables robust stable gene transfer in vertebrates. *Nat Genet* **41**, 753-761 (2009).

65. G. S. Bird, W. I. DeHaven, J. T. Smyth, J. W. Putney, Methods for studying store-operated calcium entry. *Methods* **46**, 204-212 (2008).

66. J. Weirich, L. Dumont, G. Fleckenstein-Grun, Contribution of store-operated Ca2+ entry to pH(o)-dependent changes in vascular tone of porcine coronary smooth muscle. *Cell Calcium* **35**, 9-20 (2004).

67. S. A. Kim, C. Y. Tai, L. P. Mok, E. A. Mosser, E. M. Schuman, Calcium-dependent dynamics of cadherin interactions at cell-cell junctions. *P Natl Acad Sci USA* **108**, 9857-9862 (2011).

68. S. H. Low, M. Miura, P. A. Roche, A. C. Valdez, K. E. Mostov, T. Weimbs, Intracellular redirection of plasma membrane trafficking after loss of epithelial cell polarity. *Mol Biol Cell* **11**, 3045-3060 (2000).

69. D. Willoughby, S. Wachten, N. Masada, D. M. Cooper, Direct demonstration of discrete Ca2+ microdomains associated with different isoforms of adenylyl cyclase. *J Cell Sci* **123**, 107-117 (2010).

70. C. Offord, E. Bajzer, A hybrid global optimization algorithm involving simplex and inductive search. *Lect Notes Comput Sc* **2074**, 680-688 (2001).

Acknowledgements: We are grateful to Krisztina Lór for the excellent technical assistance. We thank Junichi Nakai (RIKEN Brain Science Institute, Saitama, Japan) for providing the pN1-GCaMP2 plasmid and Robert Katona (Institute of Genetics, Biological Research Center of the Hungarian Academy of Sciences) for the pcDNA3-mCherry plasmid. The SB-CAG-Amaxa GFP vector was a kind gift of Tamás Orbán (Institute of Molecular Pharmacology, Research Centre for Natural Sciences, Hungarian Academy of Sciences). **Funding:** This work was supported by grants from OTKA (ANN-110922 and K 101064), *KTIA_AIK_12-1-2012-0025*

(AE), TRANSRAT KMR_12-1-2012-0112 (KP) and the Mayo Foundation for Medical Research and Education (AJC, ŽB, CBO, EES). **Author contributions:** AE and KP conceived the project, designed and performed the experiments, analyzed the data and wrote the manuscript; AJC, ŽB, and CBO developed the mathematical model and fitted the data; RP performed the mathematical simulations; LH and KV designed, generated and validated the plasmid constructs; EES discussed the results and implications, and critically revised the manuscript; ÁE supervised and coordinated the project. **Competing interests:** The authors declare that they have no competing interests.

Table 1. Basal activities and rate constants for binding (k_{on}) and dissociation (k_{off}) of CaM to the PMCAs. The kinetic properties are from *(16, 18)*.

PMCA	PMCA4b Slow with memory	PMCA4a Fast with no memory	PMCA2b Fast with long memory
Activity w/o CaM (% of maximum)	8.1-23	35-39	42-71
k_{on} (M^{-1} x s^{-1})	$2x10^5$	$8x10^5$	$8x10^5$
k_{off} (s^{-1})	$8x10^{-4}$	$2x10^{-2}$	$2x10^{-4}$
$K_d=k_{off}/k_{on}$ (nM)	4	25	0.25

Table 2. Theoretical Model. A: channel, AB: channel in clustered state, B: CaM-inhibited channel, P: PMCA, CaM: calmodulin, CaMh: CaM half-saturated with Ca^{2+}, Cai: cytosolic Ca^{2+} concentration, Cae: extracellular Ca^{2+} concentration, T: generic calmodulin target other than channel and pump. See text S1 for the differential equations.

A + A + A + A + A + A	<==>	AB	k_1	k'_1	(1)
AB + Cae	---->	AB + Cai	k_2		(2)
A + CaiCaM	<==>	CaiB	k_3	k'_3	(3)
Cai + P	<==>	CaiP	k_4	k'_4	(4)
CaiP	---->	Cae + P	k_5		(5)
Cai + Cai + CaM	<==>	CaiCaMh	k_6	k'_6	(6)
Cai + Cai + CaiCaMh	<==>	CaiCaM	k_7	k'_7	(7)
CaiCaM + P	<==>	PCaiCaM	k_8	k'_8	(8)
Cai + PCaiCaM	<==>	PCaiCaMCai	k_9	k'_9	(9)
PCaiCaMCai	---->	Cae + PCaiCaM	k_{10}		(10)
PCaiCaM	<==>	Cai+Cai+Cai+Cai+PCaM	k_{11}	k'_{11}	(11)
PCaM	---->	P + CaM	k_{12}		(12)
CaiCaM + T	<==>	TCaiCaM	k_{13}	k'_{13}	(13)

Table 3. Parameter values. Extracellular calcium concentration [Cae](0)= 2000 μM.

Parameter	4b	4a	2b	Reference
k_1 (s^{-1} $(\mu M)^{-5}$)	43879.2	15944.8	4217.4	this work
k'_1 (s^{-1})	0.0234	0.200	0.200	this work
k_2 (s^{-1} $(\mu M)^{-1}$)	835.2	784.6	643.9	this work
k_3 (s^{-1} $(\mu M)^{-1}$)	2.518	2.517	2.518	this work
k'_3 (s^{-1})	0.0186	0.0186	0.0186	this work
k_4 (s^{-1} $(\mu M)^{-1}$)	10	10	80	*(17, 38)* for parameters k_4, k'_4 and k_5
k'_4 (s^{-1})	50	50	50	
k_5 (s^{-1})	5.5	12	12	
k_6 (s^{-1} $(\mu M)^{-2}$)	265.8	398.7	398.7	this work
k'_6 (s^{-1})	4895.9	2447.9	2447.9	this work
k_7 (s^{-1} $(\mu M)^{-2}$)	419.3	252.9	515.1	this work
k'_7 (s^{-1})	0.0250	0.0343	0.0376	this work
k_8 (s^{-1} $(\mu M)^{-1}$)	0.2	0.8	0.8	
k'_8 (s^{-1})	0.0008	0.02	0.0002	
k_9 (s^{-1} $(\mu M)^{-1}$)	50	50	50	*(17, 19, 39)* for parameters k_8, k'_8, k_9, k'_9, k_{10}, k_{11}, k'_{11}, and k_{12}
k'_9 (s^{-1})	10	10	10	
k_{10} (s^{-1})	30	30	30	
k_{11} (s^{-1})	0.0470	0.0957	0.0314	
k'_{11} (s^{-1} $(\mu M)^{-4}$)	14.697	1.006	152.49	
k_{12} (s^{-1})	0.0331	0.0614	0.0340	
k_{13} (s^{-1} $(\mu M)^{-1}$)	1.885	14.781	1.885	this work
k'_{13} (s^{-1})	$1.175^{x}10^{-8}$	$1.124^{x}10^{-7}$	$1.142^{x}10^{-7}$	this work
$[A]_T$ μM	0.00423	0.00711	0.01126	this work
[T](0) μM	0.1355	0.2880	0.3014	this work
[Cai](0) μM	0.0767	0.0700	0.0639	this work
[P](0) μM	0.0173	0.0655	0.0356	this work
[CaM(0)] μM	0.1840	0.3598	0.1249	this work

Figure 1. Generation and characterization of a PMCA4-knockdown HeLa cell line. (**A**) PMCA abundance in control HeLa (nontransfected) and sh-PMCA4 (sh4) HeLa cells grown for 3, 5, or 7 days. Western blot analysis was performed with equal amounts (20 μg) of whole cell lysates using either the 5F10 antibody to detect both PMCA1 and PMCA4 (top) or JA3 antibody specific for PMCA4b (middle). Na,K-ATPase served as a loading control. (**B**) A representative experiment of the Ca^{2+} re-addition protocol for studying SOCE. The recordings are from sh-PMCA4 HeLa cells. Thapsigargin (Tg) inhibits SERCA, ATP stimulates release from the ER store, addition of 2 mM Ca^{2+} initiates SOCE. (**C**) SOCE-mediated Ca^{2+} transients in individual control HeLa cells expressing GCaMP2. (**D**) SOCE-mediated Ca^{2+} transients in sh-PMCA4 HeLa cells expressing GCaMP2. The data in B-D are shown as normalized values (F/F_0). The values are means ± 95% confidence interval (CI). Each panel represents >30 cells.

Figure 2. The slow and fast PMCAs generate distinct SOCE-mediated Ca^{2+} transients. (**A**, **B**) Ca^{2+} transients in HeLa cells coexpressing GCaMP2 and mCherry (mCh)-PMCA4b or mCherry-PMCA4b-LA. Top shows confocal images of the cells showing the mCherry signal. Ca^{2+} signals were monitored in individual cells positive for mCherry in response to SOCE that was induced by the re-addition protocol adding 2 mM Ca^{2+} to cells after store depletion. (**C**) Western blot analysis of whole cell lysates of HeLa cells (40 μg) and HUVECs (40 μg) stained with the pan-PMCA antibody (5F10; upper blot) and PMCA4b-specific antibody (JA3; middle blot). The first lane shows a mixture of microsomal membrane preparation from COS-7 cells (2 μg; representing PMCA1) mixed with microsomal membrane preparation from COS-7 cells transfected with the PMCA4b construct (0.05 μg; representing PMCA4b). The fourth lane shows lysates of HeLa cells transfected with mCh-PMCA4b (0.4 μg). The lower blot shows microsomal membrane preparation from COS-7 cells transfected with the PMCA2b construct (0.25 μg;

representing PMCA2b) and whole cell lysates of HUVECs (40 μg) stained with PMCA2-specific antibody (NR2). (**D**) Ca^{2+} transients in HUVECs monitored with the Ca^{2+} indicator Fluo4. SOCE was initiated by the re-addition of 0.8 mM Ca^{2+} after store depletion. (**E**) The effect of inhibition of SOCE channel with BTP2 (10 μM, 10 min) prior to store depletion and Ca^{2+} re-addition in HUVECs. (**F**, **G**) Ca^{2+} transients in HeLa cells coexpressing GCaMP2 and mCherry (mCh)-PMCA4a or mCherry-PMCA2b. Data were acquired as described in A and B. The data in A, B, D, and E represent recordings from > 15 cells. The data in F and G show the averaged Ca^{2+} signals of at least 20-30 cells represented as the mean values ± 95% CI.

Figure 3. The Ca^{2+} signal is highly sensitive to the abundance of PMCA2b but less sensitive to the abundance of the PMCA4b or PMCA4a. HeLa-GCaMP2 cells were transfected with the indicated mCherry-PMCA constructs, then SOCE was initiated with the Ca^{2+} re-addition protocol. (**A**, **B**, **C**) Relative mCherry-PMCA abundance were estimated from the fluorescence intensities of individual cells of the confocal images. We assumed that the intensity of mCherry fluorescence taken at the same acquisition parameters and settings for all constructs was directly proportional to mCherry-PMCA abundance in cells. Ca^{2+} signal peak area was quantified from Ca^{2+} transients measured after re-addition of external Ca^{2+}. Ca^{2+} peak area (in arbitrary units) was then plotted against PMCA abundance (in arbitrary units) for cells expressing the indicated mCherry-PMCAs. Each point represents a single cell and data are from two independent experiments. (**D**) Confocal images of HeLa-GCaMP2 cells transfected with mCherry-PMCA2b. The first image indicates mCh-PMCA2b (red), the others show the GCaMP2 signal (green) before (0 s) and after (10s and 50s) re-addition of Ca^{2+}. The filled arrowhead indicates a cell with a higher abundance of mCherry-PMCA2b and the open arrowhead indicates a cell with lower abundance. (**E**) Resting $[Ca^{2+}]_i$ in control and mCherry-PMCA4b- or mCherry-

PMCA2b- transfected HeLa-GCaMP2 cells. Ca^{2+} concentrations were determined according to the Hill equation [$nlogCa^{2+}=log(Y-Y_{min})/(Y_{max}-Y)+nlogK_d$, where $Y=F/F_0$; $Y_{min}=F_{min}/F_0$; $Y_{max}=F_{max}/F_0$; $K_d=1.71*10^{-7}M$; n=3.16. F_{max} and F_{min} were determined by the addition of 5 μM ionomycin and 10 mM EGTA, respectively.]. Data are shown as the mean ± SD of data points (N= 30-40 cells) from two independent experiments. (**F**) Resting $[Ca^{2+}]i$ in mCherry-PMCA2b-transfected HeLa-GCaMP2 cells plotted as a function of PMCA2b abundance.

Figure 4. SOCE-mediated Ca^{2+} transients are inhibited by SOCE channel inhibitors SKF-96365 and BTP2 in HeLa cells. (**A**) The effect of addition of SKF-96365 (50 μM) on SOCE-induced sustained elevation of $[Ca^{2+}]_i$ in mCherry-PMCA4a-transfected HeLa cells. Average trace from 34 cells is shown (mean values ± 95% CI). (**B**) The effect of addition of SKF-96365 (50 μM) on Ca^{2+} oscillations in cells expressing mCherry-PMCA4b-LA. The Ca^{2+} trace shown is representative of three separate experiments. (**C**, **D**) The effect of preincubation with BTP2 (10 μM, 10 min) prior to initiation of SOCE in HeLa cells expressing mCherry-PMCA4a (C) or mCherry-PMCA4b-LA (D). Average trace from 20-30 cells is shown (mean values ± 95% CI). Ca^{2+} signals in all panels were detected by the fluorescence of GCaMP2.

Figure 5. PMCA isoforms differentially affect SOCE induced at different extracellular Ca^{2+} concentrations. (A, B, C, D) Following store depletion, SOCE was initiated in HeLa cells expressing the indicated mCherry-PMCA constructs or in sh-PMCA4 HeLa cells by the stepwise addition of increasing $[Ca^{2+}]_e$ and intracellular $[Ca^{2+}]_i$ was followed for 5 minutes after each addition. Average traces from about 20 cells (or 8 cells for PMCA4b-LA) are shown (mean values ± 95% CI). Ca^{2+} signals in all panels were detected by the fluorescence of GCaMP2.

Figure 6. Fitting the kinetics of PMCA4b, PMCA4a, and PMCA2b to the experimental data. Data shown in Fig. 2 A, B, F, and G were fit to the model (Table 2 and text S1). The black lines correspond to the experimental data ± standard deviation (SD, dashed gray lines). The red lines represent the fits calculated by the simulations. (**A**, **B**) Data and fit of cells with PMCA4b shown on two different time scales. (**C**) Data and fit of cells with PMCA4a. (**D**) Data and fit of cells with PMCA2b.

Figure 7. Simulations of SOCE, PMCA4b activities, and $[Ca^{2+}]_i$. (A, B) Simulations of the changes of $[Ca^{2+}]_i$ and the fluxes of Ca^{2+} across the plasma membrane (J_{PMCA} and $J_{channel}$) during the first peak (A) and the subsequent Ca^{2+} oscillations (B) shown with different scales. J_{PMCA} is the flux of Ca^{2+} through PMCA into the extracellular space (J_{PMCA} = [PCaiCaMCai]*k10 + [CaiP]*k5). $J_{channel}$ is the flux of Ca^{2+} into the cytosol by the Ca^{2+} channel ($J_{channel}$ =[AB]*[Cae]*k2). (C, D) The effect of changing the association of PMCA4b with Ca^{2+}/CaM (k_8) on SOCE-generated Ca^{2+} signals. The thick blue curve with k_8=0.2 $s^{-1}\mu M^{-1}$ represents the result using the fitted kinetic value of PMCA4b. (**E**) The effect of changing the dissociation of PMCA4b with Ca^{2+}/CaM (k'_8) on SOCE-generated Ca^{2+} signals. The thick blue curve withk'_8=0.0008 s^{-1} represents the result using the fitted kinetic value of PMCA4b. (**F**) The effect of changing the abundance (P) of PMCA4b on SOCE-generated Ca^{2+} signals. The thick blue curve with P = 0.2 μM represents the curve given by the fitted parameter P of the model. Simulations were performed with DynaFit software using the model as described in Table 2 and text S1. All unstated (or unmodified) parameters used in the simulations are given in Table 3.

Figure 1.

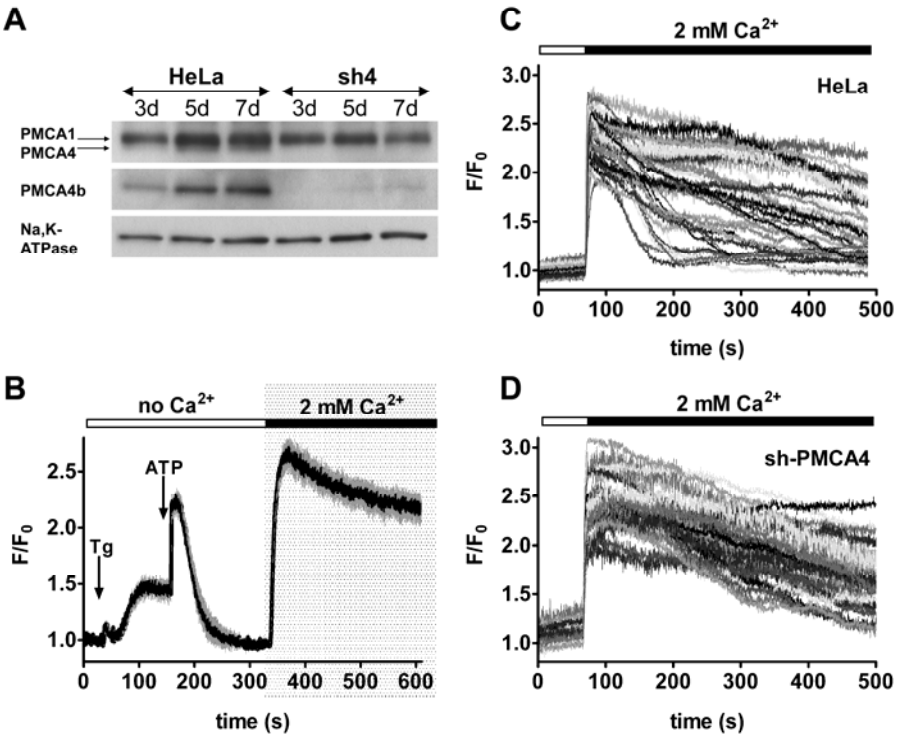

Figure 2.

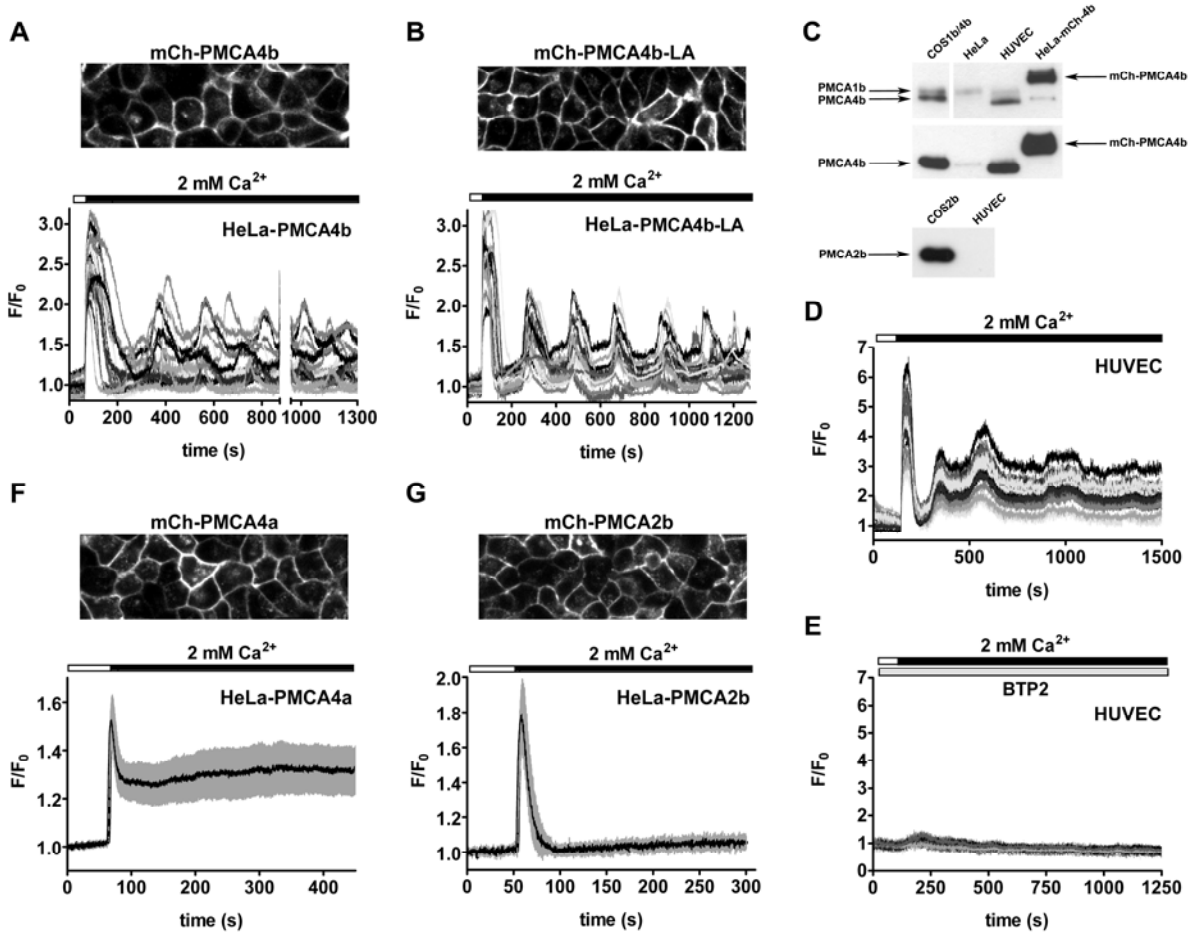

Figure 3.

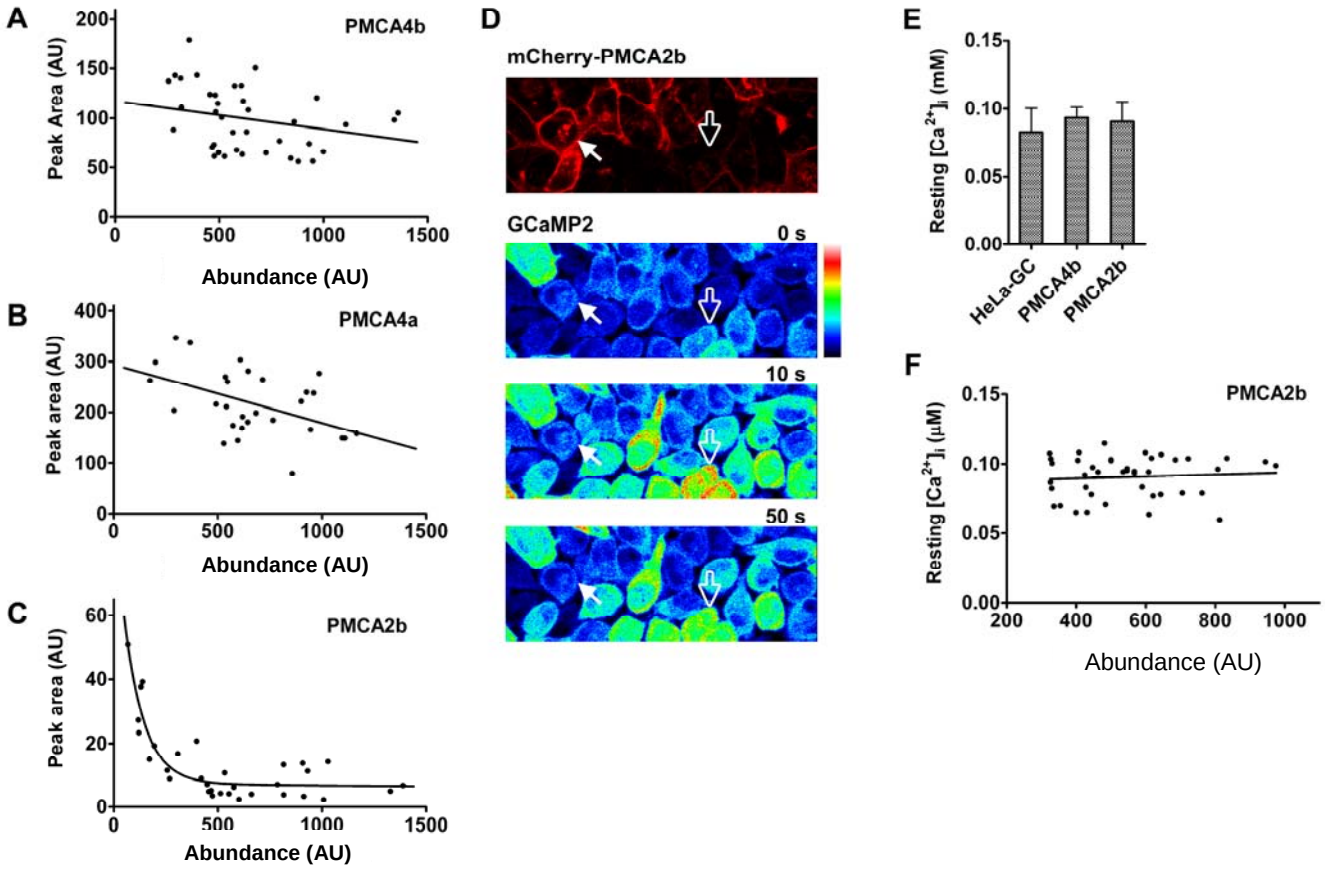

Figure 4.

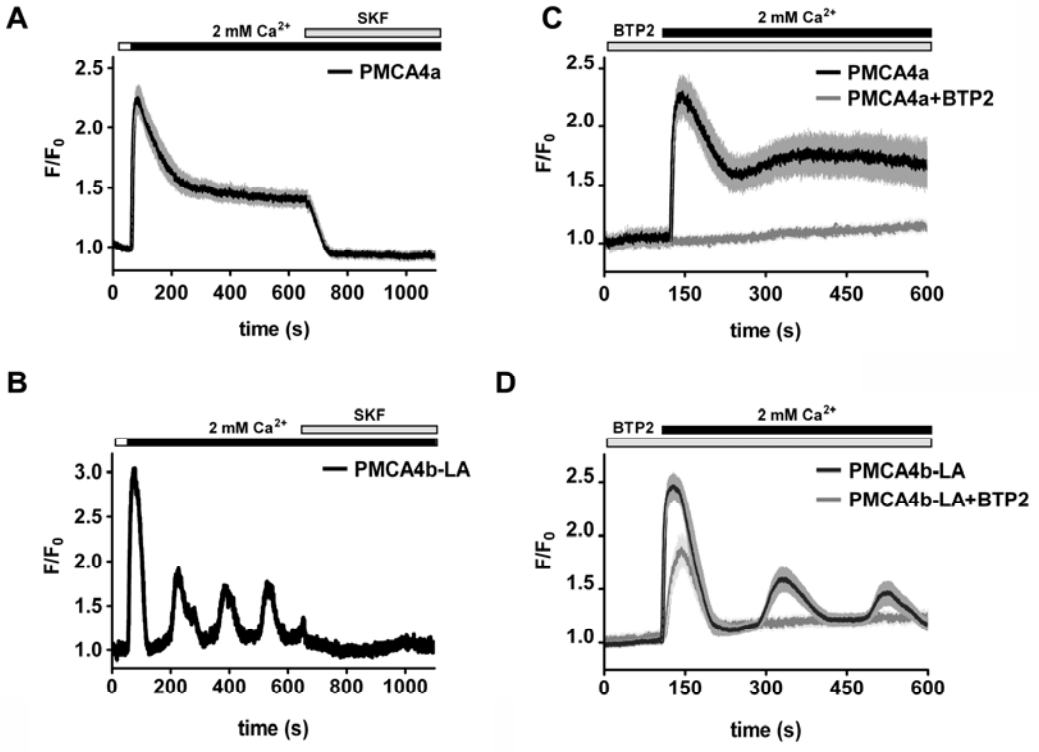

Figure 5.

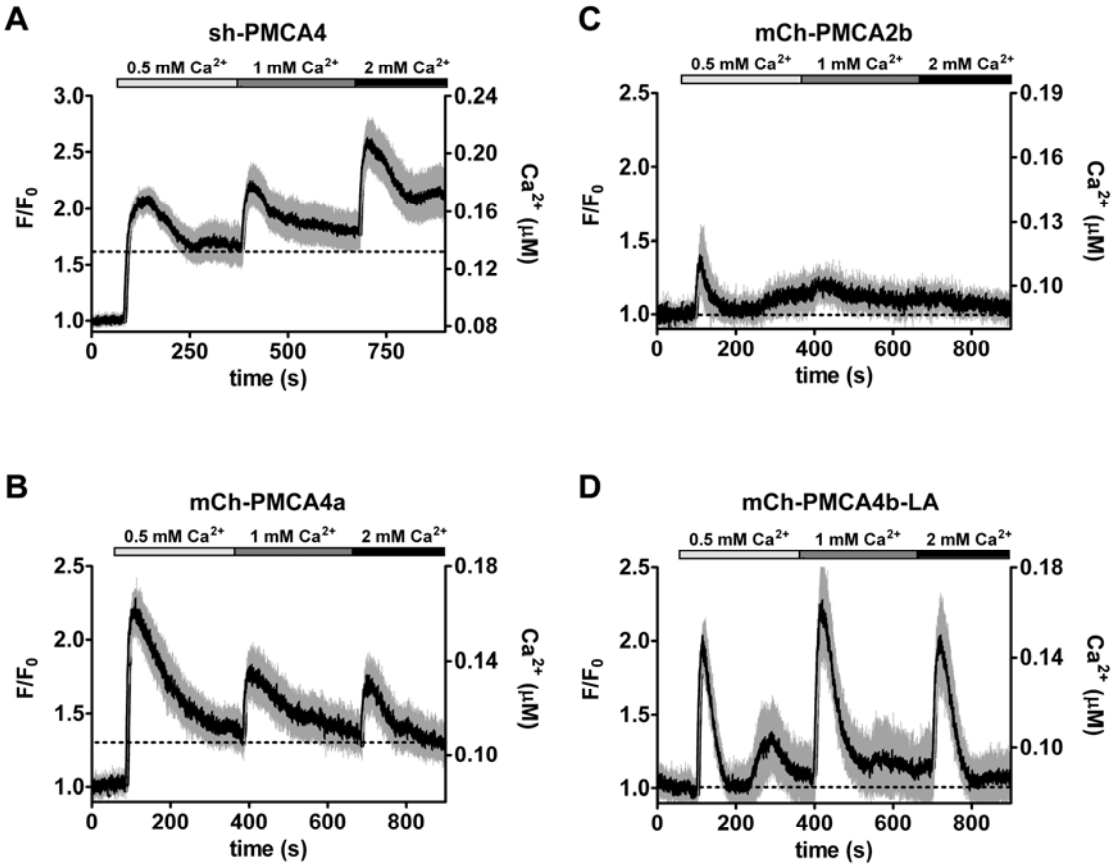

Figure 6.

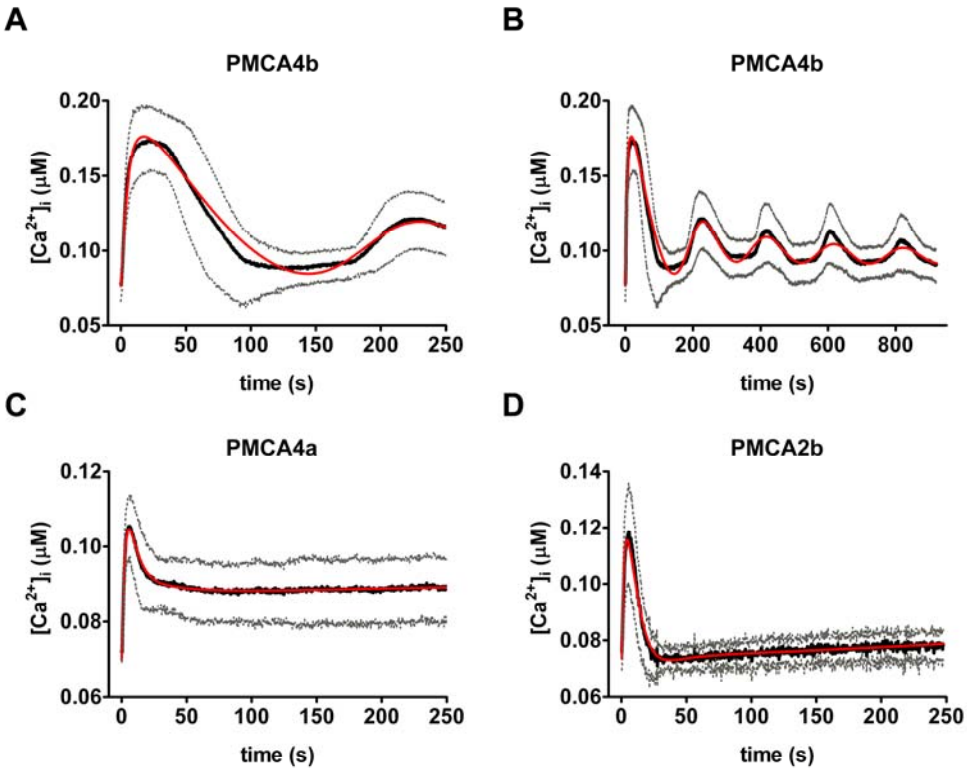

Figure 7.

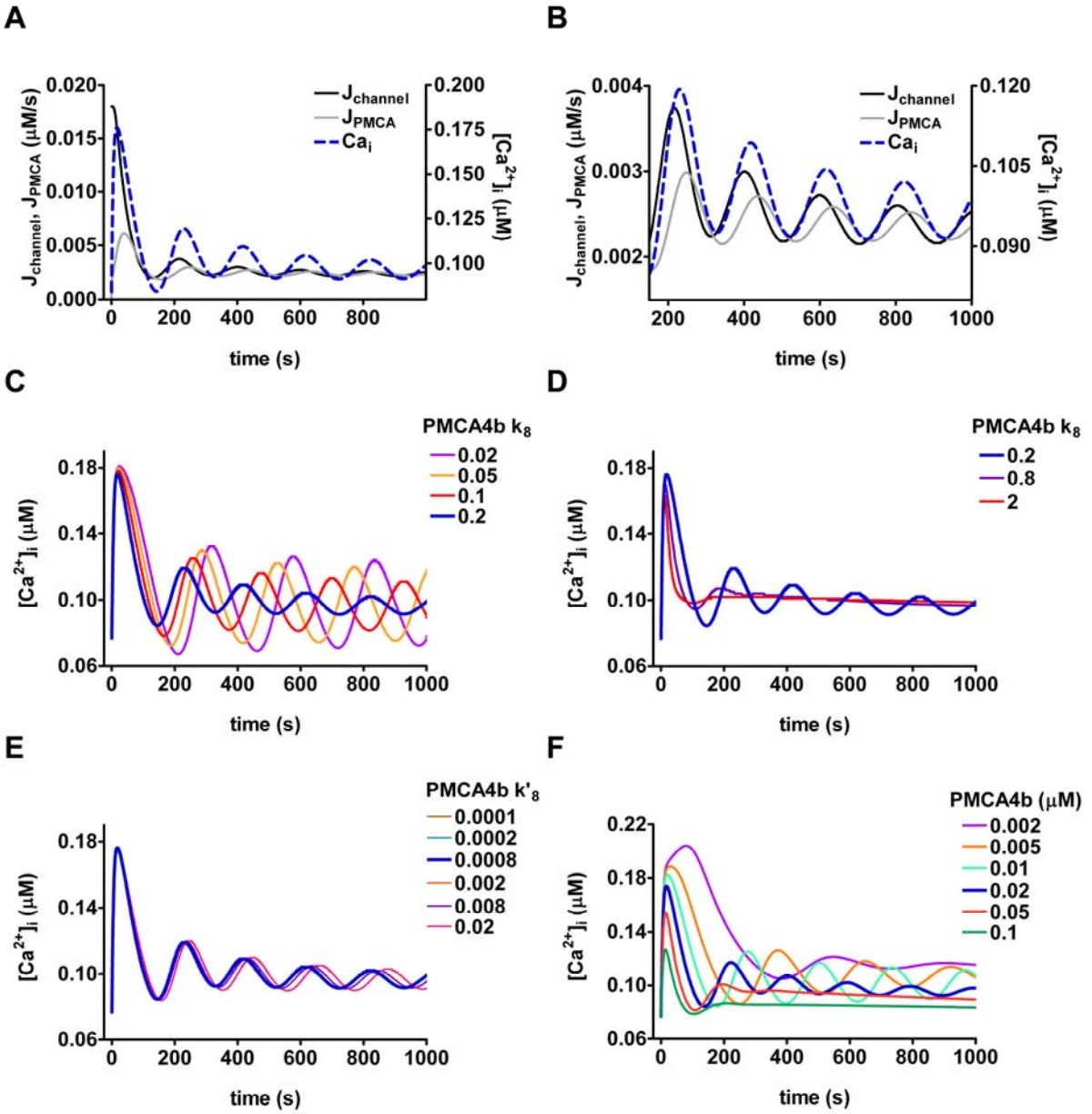
A
B
C
D
E
F
$J_{channel}$
J_{PMCA}
Ca_i
$J_{channel}$, J_{PMCA} (μM/s)
$[Ca^{2+}]_i$ (μM)
time (s)
PMCA4b k_8
0.02
0.05
0.1
0.2
0.8
2
PMCA4b k'_8
0.0001
0.0002
0.0008
0.002
0.008
0.02
PMCA4b (μM)
0.002
0.005
0.01
0.02
0.05
0.1